Dapagliflozin alleviates diabetic kidney disease via HIF-1α/HO1 mediated ferroptosis

yihui Wang
Peking University https://orcid.org/0000-0002-8511-3017
Dongyuan Chang
Peking University First Hospital
Ming-hui Zhao
Peking University First Hospital https://orcid.org/0000-0003-3340-3108
Min Chen (chenmin74@sina.com)
Peking University First Hospital

Article

Keywords: diabetic kidney diseases, SGLT2 inhibitors, dapagliflozin, hypoxia-inducible factor-1α, heme oxygenase 1, ferroptosis

Posted Date: July 15th, 2022

DOI: https://doi.org/10.21203/rs.3.rs-1745222/v1

Abstract

Background: Diabetic kidney disease (DKD) is the leading cause of end-stage kidney disease. In recent clinical trials, sodium-glucose cotransporter 2 inhibitors (SGLT2i) showed excellent renoprotection effects, but the underlying mechanism remains to be investigated. Previous studies have revealed an important role of ferroptosis, which is mediated by iron overload and lipid peroxidation, in the progression of DKD. Therefore, it is of interest to explore the effects of SGLT2i on ferroptosis in DKD due to its role in alleviating oxidative stress.

Methods: Diabetic (*db/db)* mice were administered with dapagliflozin or solvent treatment from 9 to 22 weeks of age, and were compared with non-diabetic (m/m) mice. High glucose/high fat (HG/HF) was applied to HK-2 cells, and effects of dapagliflozin on ferroptosis in HK-2 cells as well as the underlying mechanism were investigated.

Results: Typical changes of ferroptosis including massive lipid peroxidation, reduced antioxidant capability, and iron overload were found in *db/db* mice and HG/HF treated HK-2 cells. Furthermore, increased expression of hypoxia-inducible factor-1α (HIF-1α) and heme oxygenase-1 (HO1) was observed in *db/db* mice and HG/HF cultured cells as well. Dapagliflozin treatment significantly ameliorated the ferroptosis-related changes *via* inhibiting HIF-1α/HO1 axis *in vivo* and *in vitro*. Besides, downregulation of HIF-1α/HO1 axis rescued ferroptosis, while overexpression of HO1 aggravated ferroptosis induced by HG/HF in HK-2 cells. In DKD patients, the expression level of GPX4 in the kidney was significantly lower than that in healthy controls.

Conclusion: SGLT2i play a renal protective effect, at least in parts, *via* inhibiting HIF-1α/HO1 axis mediated ferroptosis.

1. Introduction

Diabetic kidney disease (DKD) develops in approximately 40% of type 2 diabetes mellitus (T2DM) patients and has become the leading cause of end-stage kidney disease (ESKD)[1, 2, 3]. Despite multifactorial risk management hyperglycemia and hypertension, the residual risk of DKD progression remains high, indicating an unmet medical need. Sodium-glucose cotransporter 2 inhibitors (SGLT2i) inhibit the coupled reabsorption of sodium and glucose from the proximal tubule, reducing glucose reentry from tubular fluid into the bloodstream. Many recent clinical trials showed the renoprotectionve effects of SGLT2i in patients with T2DM[4, 5, 6, 7], but the underlying mechanisms were not fully clear.

Multiple factors, including hemodynamic dysfunction, oxidative stress, hypoxia, and inflammation contribute to the development and progression of DKD[8]. Ferroptosis is a form of regulated cell death culminating with the accumulation of redox-active iron and iron-dependent lipid peroxidation [9]. Oxidative stress is crucial in ferroptosis for reactive oxygen species (ROS) generation and polyunsaturated fatty acids (PUFAs) peroxidation. Glutathione peroxidase 4 (GPX4), solute carrier family 7 member 11

(SLC7A11), and nuclear factor erythroid 2-related factor 2 (NRF2) function as negative regulators of ferroptosis by relieving ROS accumulation through antioxidant capacity[10, 11, 12], while transferrin receptor (TFRC), NADPH oxidase, and p53 act as positive regulators of ferroptosis by stimulating iron uptake and/or promoting ROS production[13, 14]. Previous studies suggested that ferroptosis is involved in the pathogenesis of DKD by bioinformatics analysis as well as *in vivo* and *in vitro* experiments[15, 16, 17]. Anti-oxidative stress is a prominent pathway related to the renoprotective effects of SGLT2i[18, 19, 20]. Therefore, it is reasonable to speculate that SGLT2i play a renoprotective role *via* inhibiting ferroptosis.

Hypoxia-inducible factor-1α (HIF-1α), which binds to hypoxia response elements (HREs; 5'-RCGTG-3'), regulates a variety of genes including iron homeostasis associated genes such as heme oxygenase-1 (HO1, catalyzing the rate-limiting heme oxidation to biliverdin, carbon monoxide, and free ferrous iron[21, 22]) and TFRC[23, 24], and thus makes it a key regulator of ferroptosis. Although Feng X's study found that ferroptosis could aggravate albuminuria, damage renal tubules, and enhance renal fibrosis through HIF-1α/HO-1 pathway in diabetic mice[25], several lines of evidence showed the survival-promoting effects of HIF-1α and HO1 on inhibiting ferroptosis in other models[26, 27, 28, 29, 30, 31]. Moreover, Jiang N's study revealed that HIF-1α exerted a protective effect against tubular injury by improving mitochondrial quality in DKD through HO1 upregulation[32]. Given the controversial role of HIF-1α and HO1 in ferroptosis and DKD, it is of interest to elucidate the renoprotective effects of SGLT2i in DKD *via* regulating ferroptosis by HIF-1α/HO1 axis since SGLT2i can attenuate hypoxia as well as HIF-1α accumulation *in vivo* and *in vitro*[33, 34].

2. Materials And Methods

2.1 Patients and samples

Twenty patients with T2DM and biopsy-proven DKD, diagnosed from January 2017 to December 2017 in Peking University First Hospital[35], were enrolled in this study. T2DM was defined according to the criteria proposed by the American Diabetes Association in 2017[36]. None of the patients had coexisting non-diabetes-related renal disease. DKD was defined as previously described[35]. Healthy control kidney samples were obtained from healthy kidney poles of individuals (n = 10) receiving tumor nephrectomies without diabetes or other kidney diseases. All healthy control kidney samples were confirmed by pathological examinations including immunofluorescence, light microscopy, and electron microscopy. Clinical data of the patients at the time of renal biopsy was systematically recorded. Biopsies were scored independently by two experienced pathologists respectively. Interstitial fibrosis and tubular atrophy (IFTA) scores were assessed semi-quantitatively based on the proportion of the tubulointerstitial compartment affected (0, none; 1, < 25%; 2, 25–50%; 3, > 50%)[35]. The investigation was conducted according to the Declaration of Helsinki and was approved by the Ethics Committee of Peking University First Hospital (2017 − 1280). Written informed consent was obtained from each participant at renal biopsy.

2.2 Animal experimentation

Wild-type and *db/db* mice (male, 8 weeks old) inbred on C57BLKS/J background were purchased from Gempharmatech Co., Ltd (Nanjing, China). The mice were randomly allocated into three groups after one-week acclimatization: a wild-type group (m/m, n = 7), a *db/db* group receiving 1 mg/kg/day dapagliflozin (AstraZeneca Pharmaceuticals LP, solving in 0.5% methylcellulose) treatment (*db/db*-Dapa, n = 7) and a *db/db* group receiving solvent as a vehicle (*db/db*-Veh, n = 6). During the 13-week treatment, body weight was monitored every week. Fasting blood glucose (FBG) was obtained at week0, 4, 8, and 13. The 24-h urine was collected using the metabolic cage to measure urinary albumin (E99-134; Bethyl Laboratories, Montgomery, TX, USA) and creatinine (C011; Nanjing Jiancheng, Nanjing, China) at week0, 4, and 13. Urinary HO1 levels were measured at week0 and 13 (ab205524; Abcam, Cambridge, MA, USA). Kidney tissues were collected before the time of euthanization and preserved for examination. All animal experiments were approved by the Laboratory Animal Ethics Committee of Peking University First Hospital (J202138).

2.3 Renal histology

Staining of kidney sections was performed using periodic acid Schiff (PAS; K1433; BioVision, CA, USA). Glomerular area was measured by tracing around the perimeter of the glomerular tuft. The mesangial matrix expansion area was assessed from the images of glomeruli and presented as a proportion of PAS-stained per glomerular cross-sectional area. The tubulointerstitial injury index was determined by assessing the extent and severity of tubular dilation, atrophy, and loss of tubular cells. Twenty images of a kidney section (magnification ×400) were scored as follows: 0 for no injury, 1 for < 25%, 2 for 25–50%, 3 for 50–75%, and 4 for > 75% tubulointerstitial injury[35]. Quantitation analyses were performed on Image-Pro Plus software V.6.0 (Media Cybernetics, Bethesda, MD).

2.4 Immunohistochemistry (IHC)

Formalin-fixed paraffin-embedded kidney tissue sections were blocked by 3% bovine serum albumin (BSA, A1933; Sigma-Aldrich, St Louis, MO, USA) after heat-induced epitope retrieval, and stained with anti-HO1 antibody (ab52947; Abcam), anti-TFRC antibody (ab84036; Abcam), or anti-GPX4 antibody (ab125066; Abcam) overnight at 4° C, respectively. Subsequently, an HRP-DAB system (PV-9002; ZLI-9018; ZSBIO, Beijing, China) was used for color development. Twenty images (magnification ×400) of each section were assessed by Image-Pro Plus.

2.5 Transmission electron microscopy

The renal cortical tissues of mice were fixed in 3% glutaraldehyde and further sample handling was performed by the Laboratory of Electron Microscopy, Peking University First Hospital. Imaging was performed by a Hitachi HT7800 transmission electron microscope (Hitachi, Japan). The measurement of glomerular basement membrane (GBM) thickness and mitochondria analysis of renal tubular epithelial cells was processed using Image-pro plus.

2.6 Cell culture

HK-2 human kidney proximal tubular cells (American Type Culture Collection, Rockville, MD) were cultured in DMEM nutrient mix F12 (11330-032; Gibco, Carlsbad, CA, USA) supplemented with 10% fetal bovine serum (10099141; Gibco, Australia), 1% penicillin-streptomycin (V900929; Sigma-Aldrich) at 37℃, 95% humidity, and 5% CO_2. Cells were seeded in 6, 12 or 96-well plates, and cells were exposed to different treatments for 24, 48 or 72h, including 30 mM D-glucose (high glucose; HG) (G8270, Sigma-Aldrich) or D-mannitol (Man) (M4125, Sigma-Aldrich), 200 μM palmitic acid (high fat; HF) (P0500, Sigma-Aldrich) or BSA (A9576, Sigma-Aldrich), 20 μM dapagliflozin (Dapa) (HY-10450; MedChemExpress (MCE), NJ, USA), 20 nM PX-478 (HY-10231; MCE), 80 μM hemin (HY-19424; MCE), 5 μM zinc protoporphyrin (Znpp) (HY-101193; MCE), 1 mM dimethyloxallyl glycine (DMOG) (HY-B0988; MCE), 50 μM deferoxamine mesylate (DFO) (HY-B0988; MCE), 2 μM erastin (HY-15763; MCE), 5 μM RSL3 (HY-100218A; MCE) and 1 μM ferrostatin-1 (Fer-1) (HY-100579; MCE), respectively.

2.7 Cell viability assay

Cell viability was measured using Cell Counting Kit-8 (CCK8-100; Dojindo, Kumamoto, Japan) according to the manufacturer's instructions.

2.8 Iron and malondialdehyde (MDA) assay

Intracellular ferrous iron (Fe^{2+}) was assessed by fluorescent probe FerroOrange (F374; Dojindo) *via* fluorescence-activated cell sorter (FACS) analysis using BD FACSVerse (BD biosciences, NJ, USA), while total iron concentration was measured by Iron detection kit (TC1015; Leagene, Bejing, China). MDA concentrations were determined by the Micro Malondialdehyde Assay Kit (BC0025; Solarbio, Beijing, China).

2.9 Quantification of lipid peroxidation

HK-2 cells were incubated with 2.5 μM C11-BODIPY$^{581/591}$ (D3861; Thermofisher Scientific, MA, USA) for 45 min at 37℃. Then cells were collected and washed once with PBS followed by FACS. Fluorescence intensity was analyzed using FlowJo_V7 software.

2.10 Assessment of mitochondrial activity

Mitochondrial activity in HK-2 cells was assessed (C1035; Beyotime, Beijing, China) *via* FACS analysis or confocal laser scanning microscope. The fluorescence intensity of FACS was analyzed using FlowJo_V7 software.

2.11 Quantitative real-time PCR (qRT-PCR)

Total RNA was extracted (DP441; Tiangen, Beijing, China) and reverse transcribed into cDNA (4374966; Applied Biosystems, MA, USA). The qRT-PCR analysis was carried out in an ABI Prism 7500 sequence detection system using SYBR Green Master Mix (A25742; Applied Biosystems). Primers are listed in Table S1.

2.12 Western blot

Total protein was extracted, and nucleoprotein and cytoplasmic proteins from HK-2 cells were isolated (P0027; Beyotime). Protein was separated using 10% SDS-PAGE and transferred to PVDF membranes, which were probed with primary antibodies against HIF-1α (10006421; Cayman, USA), TFRC (13-6800; Thermo Scientific) GPX4 (ab125066; Abcam) and HO1 (10701-1-AP; Proteintech, CHI, USA). β-actin (sc-47778; Santa Cruz Biotechnology, CA, USA) and histone 3 (4499T; Cell Signaling Technology, MA, USA) were used as internal controls. Protein was visualized on autoradiographic film using an ECL Plus Western blot detection system (GE Healthcare).

2.13 Bioinformatic analysis

The transcriptome sequencing and analysis were conducted by OE Biotech Co., Ltd. (Shanghai, China). Raw data were processed using Trimmomatic[37]. After removing the low-quality reads, clean data were mapped to the reference genome using hisat2[38]. FPKM[39] value was calculated using cufflinks[40], and the read counts were obtained by htseq-count[41]. Differentially expressed genes (DEGs) were identified using DESeq[42] R package, and $p < 0.05$ and fold change > 2 *or* fold change < 0.5 was set as the threshold for significantly differential expression. KEGG[43] pathway enrichment analysis of DEGs was performed using the Cluster Profiler R package.

2.14 Statistical analysis

Normally distributed data were presented as mean ± standard deviation (SD), and non-normally distributed data were presented as median and interquartile range (IQR). Groups were compared using unpaired two-tailed Student's t-tests or one-way analysis of variance (ANOVA) as appropriate. Pearson or Spearman correlation analysis was used to evaluate the association between immunohistochemistry staining intensity (IOD/area) and clinicopathological parameters as appropriate. A p value less than 0.05 was considered statistically significant (*$p < 0.05$, **$p < 0.01$, ***$p < 0.001$). All the results were plotted using GraphPad Prism 8 software.

3. Results

3.1 Dapagliflozin ameliorated DKD in *db/db* mice

The vehicle-treated *db/db* mice showed significantly higher body weight, 24-h urinary albumin excretion, urine albumin-to-creatinine ratio (uACR), and FBG than m/m mice (43.5 ± 8.70 *vs.* 28.8 ± 1.02 g, $p < 0.001$; 11.7 ± 5.32 *vs.* 2.9 ± 1.46 mg/24h, $p < 0.01$; 768.7 ± 372.53 *vs.* 20.5 ± 8.82 μg/mg, $p < 0.001$; 32.0 ± 3.18 *vs.* 7.5 ± 2.30 mmol/l, $p < 0.001$; respectively) (Table 1). Dapagliflozin-treated *db/db* mice showed significant amelioration of 24-h urinary albumin excretion, uACR and FBG compared with vehicle-treated *db/db* mice

(6.7 ± 2.03 *vs.* 11.7 ± 5.32 mg/24h, $p < 0.05$; 289.2 ± 118.32 *vs.* 768.7 ± 372.53 μg/mg, $p < 0.01$; 19.4 ± 5.26 *vs.* 32.0 ± 3.18 mmol/l, $p < 0.001$; respectively) (Table 1). No obvious adverse event was found in any experimental group.

Table 1
Laboratory data of mice

	m/m mice	vehicle-treated *db/db* mice	dapagliflozin-treated *db/db* mice
Body weight, g	28.8 ± 1.02	43.5 ± 8.70*	51.4 ± 6.53
Water intake, ml/24h	4.6 ± 0.91	25.9 ± 10.72*	26.4 ± 5.50
Food intake, g/24h	4.5 ± 1.04	12.8 ± 3.22*	12.1 ± 4.11
Urine volume, ml/24h	0.9 ± 0.51	15.4 ± 9.00*	15.3 ± 5.37
FBG, mmol/l	7.5 ± 2.30	32.0 ± 3.18*	19.4 ± 5.26#
Triglyceride, mmol/l	0.8 ± 0.15	1.7 ± 0.48*	1.0 ± 0.21#
uACR, μg/mg	20.5 ± 8.82	768.7 ± 372.53*	289.2 ± 118.32#
Urine albumin, mg/24h	2.9 ± 1.46	11.7 ± 5.32*	6.7 ± 2.03#

FBG, fasting blood glucose; uACR, urine albumin-to-creatinine ratio. The continuous data were expressed as mean ± SD.* $p < 0.01$ *vs.* m/m mice; # $p < 0.05$ vs. vehicle-treated *db/db* mice.

PAS staining analysis showed that dapagliflozin-treated *db/db* mice manifested alleviated histological changes in kidneys, including glomerular size, mesangial matrix expansion, and tubulointerstitial lesions (Fig. 1A-D). The ultrastructural analysis demonstrated that dapagliflozin-treated *db/db* mice had significant improvement in glomerular basement membrane thickness, as compared with vehicle-treated db/db mice (Fig. 1E and F). These *in vivo* findings suggested dapagliflozin significantly ameliorated DKD of *db/db* mice.

3.2 Dapagliflozin alleviated renal ferroptosis in *db/db* mice

The level of MDA which increased in kidney cortex of vehicle-treated *db/db* mice was significantly alleviated in dapagliflozin-treated *db/db* mice, indicating the decreased lipid peroxidation upon dapagliflozin treatment (Fig. 1G). GPX4, which mainly expressed in tubulointerstitium, significantly increased in kidney cortex of dapagliflozin-treated *db/db* mice compared with vehicle-treated *db/db* mice (Fig. 1H-K).

Transmission electron microscopy revealed that typical changes of mitochondria in ferroptosis in kidney tubular epithelial cells including ruptured mitochondrial membrane and disappeared mitochondrial

cristae[44], were improved in dapagliflozin-treated *db/db* mice, as compared with vehicle-treated *db/db* mice (Fig. 1E). Consistently, the form factor and aspect ratio of mitochondria were improved by dapagliflozin treatment (Fig. 1Land M).

TFRC upregulated in vehicle-treated *db/db* mice was significantly alleviated in dapagliflozin-treated *db/db* mice (Fig. 1H-K). Total iron concentration significantly decreased in dapagliflozin-treated *db/db* mice compared with vehicle-treated *db/db* mice (Fig. 1N). Collectively, dapagliflozin ameliorated renal ferroptosis in *db/db* mice.

3.3 Dapagliflozin downregulated HIF-1α/HO1 axis in *db/db* mice.

Kidney cortical tissues of mice were isolated for metabolomics analysis. 49 and 10 differential metabolites were found in *db/db*-vehicle *vs.* m/m group and *db/db*-dapagliflozin *vs. db/db*-vehicle group respectively (Fig. 2A and B). Arachidonic acid signaling was upregulated in vehicle-treated *db/*db mice compared with m/m and dapagliflozin-treated db/db mice, and lipid peroxidation products derived from arachidonic acid have been claimed as the proximate executioners of ferroptosis[12, 45] (Fig. 2C and D).

In RNA-Seq analysis, there were 2187 and 285 DEGs in *db/db*-vehicle *vs.* m/m group and *db/db*-dapagliflozin *vs. db/db*-vehicle group respectively (Fig. 2E). HO1, a key regulator of oxidative stress and strongly associated with ferroptosis, stood out among a group of DEGs in *db/db*-dapagliflozin *vs. db/db*-vehicle group (Fig. 2F). KEGG pathway enrichment analysis based on the RNA-Seq data showed that arachidonic acid (endocannabinoid) signaling was simultaneously enriched in *db/db*-vehicle *vs.* m/m group and *db/db*-dapagliflozin *vs. db/db*-vehicle group, which was consistent with the metabolomics analysis (Fig. S1A and B).

We verified the RNA-Seq results on protein level and confirmed that dapagliflozin treatment led to a remarkable reduction of HIF-1α and HO1 expression, as compared with vehicle-treated *db/db* mice (Fig. 3A-D). Meanwhile, the urinary HO1 level was also significantly reduced in dapagliflozin-treated *db/db* mice compared with vehicle-treated *db/db* mice (Fig. 3E). These results suggested that HIF-1α/HO1 axis may be associated with the ferroptosis inhibition effects of dapagliflozin in *db/db* mice.

3.4 Dapagliflozin relieved HG/HF induced ferroptosis by downregulating HIF-1α/HO1 axis *in vitro*

The viability of HK2 cells with HG/HF treatment was significantly decreased compared with control group (Man/BSA and vehicle treated cells), which was rescued by dapagliflozin, DFO (ferroptosis inhibitor), and Fer-1 (ferroptosis inhibitor) (Fig. 4A). Dapagliflozin restored the cell viability reduction induced by RSL3, a ferroptosis inducer by inhibiting GPX4 activity[46] (Fig. 4A).

Significantly reduced mitochondrial activity (Fig. 4B and C) was found in HG/HF group compared with control group. Lipid peroxidation level (Fig. 4D) increased, while GPX4 expression decreased upon HG/HF

treatment (Fig. 4E-G). These alterations were accompanied by increased expression of HIF-1α (in both whole cell and nucleus), HO1 and TFRC (Fig. 4E-G) as well as elevated iron levels (Fig. 4H-J).

Under HG/HF condition, cells in dapagliflozin group have significant restoration of the cell viability (Fig. 4A), mitochondrial activity (Fig. 4B and C), and GPX4 expression compared with vehicle group (HG/HF and solvent treated cells) (Fig. E-G). The lipid peroxidation level (Fig. 4D) and iron concentration (Fig. 4H-J) were significantly lower in dapagliflozin group than in vehicle group.

Under HG/HF condition, overexpression of HIF-1α by DMOG (Fig. 5A and B) weakened the effects of dapagliflozin, evidenced by reduced cell viability (Fig. 5C), mitochondrial activity (Fig. 5D and E) and GPX4 expression (Fig. 5A, B and F), as well as enhanced iron overload (Fig. 5G-I) and lipid peroxidation (Fig. 5J) in dapagliflozin and DMOG treated cells compared with dapagliflozin treated cells. Moreover, overexpression of HO1 by hemin (Fig. 5A and B) reversed the effects of PX-478 (HIF-1α inhibitor), as evidenced by aggravated ferroptosis in cells treated with PX-478 and hemin compared with cells with PX-478 treatment alone (Fig. 5A-J).

These data suggested that dapagliflozin alleviated HG/HF induced ferroptosis *via* downregulating HIF-1α/HO1 axis *in vitro*.

3.5 Inhibition of HIF-1α/HO1 axis rescued HG/HF induced ferroptosis *in vitro*

Under HG/HF condition, inhibition of HIF-1α or HO1 (by PX-478 and Znpp respectively) restored the cell viability impaired in vehicle group (Fig. 5C). PX-478 and Znpp also improved mitochondria activity (Fig. 5D and E) and reduced lipid peroxidation level (Fig. 5J) compared with vehicle group. Upregulation of GPX4 (Fig. 5A, B and F) and relieved iron overload (Fig. 5G-I) were also observed in PX-478 and Znpp treated cells.

Interestingly, TFRC was upregulated in DMOG and Znpp treatment but not in PX-478 treatment whether with or without hemin (Fig. 5A, B and F), which indicated HO1 and TFRC were regulated by HIF-1α while GPX4 was regulated by HO1. Collectively, these findings showed the inhibition of the HIF-1α/HO1 axis could suppress ferroptosis of HK-2 cells induced by HG/HF.

3.6 Ferroptosis was associated with the disease severity in DKD patients

We further analyzed the correlation between ferroptosis and disease severity in DKD patients (general data in Table S2). GPX4 level in kidney tubulointerstitium was significantly lower in DKD patients than in healthy controls (Fig. 6A and B), while HO1 and TFRC levels were significantly higher in kidney tubulointerstitium of DKD patients than in healthy controls (Fig. 6A and B). HO1 level positively correlated with serum creatinine (Scr) ($r = 0.54$, $p < 0.05$; Fig. 6C) and negatively correlated with estimated glomerular filtration rate (eGFR) ($r = -0.59$, $p < 0.01$; Fig. 6D), and GPX4 level negatively correlated with Scr ($r = -0.63$, p

< 0.01; Fig. 6E) and positively correlated with eGFR (r = 0.69, $p < 0.001$; Fig. 6F). These data suggested that ferroptosis was associated the disease severity of DKD in patients.

4. Discussion

SGLT2i have emerged as a promising antidiabetic drug with renoprotection in T2DM patients[47], and the role of ameliorating oxidative stress in SGLT2i mediated renal protection has aroused increasing attention recently[19]. In the current study, we found that dapagliflozin relieved ferroptosis in *db/db* mice and HK-2 cells, including lipid peroxidation products accumulation, weakened antioxidant capacity and iron overload, by downregulating the HIF-1α/HO1 axis. In addition, we found that HO1 and GPX4 in kidney tubulointerstitium significantly correlated with the disease severity in DKD patients.

In diabetic kidneys, enhanced glucose reabsorption by renal proximal tubular cells (RPTCs) (*via* SGLT2) increases oxygen consumption and predisposes the renal cortex to hypoxia[48], and increased HIF-1α expression in RPTCs suggested that hypoxia of renal tubules was a hallmark of DKD[49, 50]. Some studies showed the pathogenic role of HIF-1α in DKD[51, 52, 53], while others found that modulation of metabolic disorders and inflammation in diabetic mice by hypoxia-inducible factor stabilizers (prolyl hydroxylase inhibitors) was protective[54, 55]. Adaptive upregulation of HIF-1α under hypoxia could be protective to a certain degree, while overactivation of HIF-1α would lead to tissue damage. In addition, except HIF-1α prolyl hydroxylase inhibitors also stabilize HIF-2α[55]. HIF-2α played a protective role in DKD by inhibiting inflammation and fibrosis[56], which should be taken into consideration of studies of prolyl hydroxylase inhibitor. SGLT2i improved hypoxia, which explained the prevention of HIF-1α accumulation by SGLT2i mechanistically.

Accumulation of HIF-1α in DKD induces the expression of HO1 and TFRC and regulates iron metabolism[57]. Although previous evidence indicated that HO1 had protective effects in DKD[58, 59, 60], several studies found elevated HIF-1α and HO1 levels in kidneys of diabetic models[25, 61]. HO1 help attenuate oxidative stress in the early stage, while continuous HO1 upregulation will trigger ferroptosis[62, 63], which indicates that the effect of HO1 in DKD may depend on different pathological conditions. We found that upregulation of the HIF-1α/HO1 axis promoted ferroptosis *in vivo* and *in vitro*, and inhibition of the HIF-1α/HO1 axis alleviated ferroptosis. Moreover, upregulation of the HIF-1α/HO1 axis weakened the ferroptosis-relieving effect of dapagliflozin, which suggested alleviated iron overload by SGLT2i through the HIF-1α/HO1 axis could, at least to some extent, explain its renoprotective effects.

Cyst(e)ine/glutathione (GSH)/GPX4 signaling axis constitutes the predominant ferroptosis defense system[10, 64, 65]. However, we found dapagliflozin could rescue ferroptosis induced by RSL3 but not erastin (ferroptosis inducer by inhibiting SLC7A11 activity) in HK-2 cells (Fig. S2), which indicated that dapagliflozin inhibits ferroptosis by regulating GPX4 expression rather than SLC7A11. GPX4 utilizes GSH as its cofactor to prevent ferroptosis by eliminating membrane phospholipid hydroperoxides and maintaining the integrity of phospholipid bilayers[66]. GPX4 deficiency is regarded as one of the

biomarkers of ferroptosis, and GPX4 depletion caused massive renal tubular epithelial cells to undergo ferroptosis[10, 67, 68]. Dapagliflozin could reverse the GPX4 reduction *in vivo* and *in vitro*, which suggested that the restored antioxidant capacity against lipid peroxidation caused by the iron overload of SGLT2i was also necessary for its renoprotective role.

There were many other pathways with significant changes in metabolomics and RNA-Seq (Fig. 2C and D; Fig. S1), so more detailed insights are needed to elaborate the effects of these pathways in the renoprotective effect of SGLT2i.

In conclusion, dapagliflozin alleviated DKD progression by mitigating ferroptosis through HIF-1α/HO1 axis (Fig. 7). The present study explained the renoprotective effect of SGLT2i from a new angle.

Declarations

Acknowledgments

We are grateful to the Laboratory Animal Center of Peking University First Hospital for the technical support of this study.

Competing Interests

All the authors have nothing to disclose.

Funding

This research was funded by the National Natural Science Found [grant number 82070748, 82090020, and 82090021]; CAMS Innovation Fund for Medical Sciences [grant number 2019-I2M-5-046]; and Hengrui Pharmacy.

References

1. Alicic RZ, Rooney MT, Tuttle KR. Diabetic Kidney Disease: Challenges, Progress, and Possibilities. Clinical journal of the American Society of Nephrology: CJASN 2017, **12**(12): 2032–2045.
2. Nespoux J, Vallon V. Renal effects of SGLT2 inhibitors: an update. Current opinion in nephrology and hypertension 2020, **29**(2): 190–198.
3. Warren AM, Knudsen ST, Cooper ME. Diabetic nephropathy: an insight into molecular mechanisms and emerging therapies. Expert opinion on therapeutic targets 2019, **23**(7): 579–591.
4. Wanner C, Inzucchi SE, Lachin JM, Fitchett D, von Eynatten M, Mattheus M, *et al.* Empagliflozin and Progression of Kidney Disease in Type 2 Diabetes. The New England journal of medicine 2016, **375**(4): 323–334.
5. Perkovic V, Jardine MJ, Neal B, Bompoint S, Heerspink HJL, Charytan DM, *et al.* Canagliflozin and Renal Outcomes in Type 2 Diabetes and Nephropathy. The New England journal of medicine 2019,

380(24): 2295–2306.

6. Neuen BL, Young T, Heerspink HJL, Neal B, Perkovic V, Billot L, *et al.* SGLT2 inhibitors for the prevention of kidney failure in patients with type 2 diabetes: a systematic review and meta-analysis. The lancet Diabetes & endocrinology 2019, **7**(11): 845–854.
7. Vergara A, Jacobs-Cachá C, Soler MJ. Sodium-glucose cotransporter inhibitors: beyond glycaemic control. Clinical kidney journal 2019, **12**(3): 322–325.
8. Lin YC, Chang YH, Yang SY, Wu KD, Chu TS. Update of pathophysiology and management of diabetic kidney disease. Journal of the Formosan Medical Association = Taiwan yi zhi 2018, **117**(8): 662–675.
9. Zheng J, Conrad M. The Metabolic Underpinnings of Ferroptosis. Cell metabolism 2020, **32**(6): 920–937.
10. Friedmann Angeli JP, Schneider M, Proneth B, Tyurina YY, Tyurin VA, Hammond VJ, *et al.* Inactivation of the ferroptosis regulator Gpx4 triggers acute renal failure in mice. Nature cell biology 2014, **16**(12): 1180–1191.
11. Yang WS, Kim KJ, Gaschler MM, Patel M, Shchepinov MS, Stockwell BR. Peroxidation of polyunsaturated fatty acids by lipoxygenases drives ferroptosis. Proceedings of the National Academy of Sciences of the United States of America 2016, **113**(34): E4966-4975.
12. Kagan VE, Mao G, Qu F, Angeli JP, Doll S, Croix CS, *et al.* Oxidized arachidonic and adrenic PEs navigate cells to ferroptosis. Nature chemical biology 2017, **13**(1): 81–90.
13. Stockwell BR, Friedmann Angeli JP, Bayir H, Bush AI, Conrad M, Dixon SJ, *et al.* Ferroptosis: A Regulated Cell Death Nexus Linking Metabolism, Redox Biology, and Disease. Cell 2017, **171**(2): 273–285.
14. Jiang L, Kon N, Li T, Wang SJ, Su T, Hibshoosh H, *et al.* Ferroptosis as a p53-mediated activity during tumour suppression. Nature 2015, **520**(7545): 57–62.
15. Li S, Zheng L, Zhang J, Liu X, Wu Z. Inhibition of ferroptosis by up-regulating Nrf2 delayed the progression of diabetic nephropathy. Free radical biology & medicine 2021, **162**: 435–449.
16. Wang Y, Bi R, Quan F, Cao Q, Lin Y, Yue C, *et al.* Ferroptosis involves in renal tubular cell death in diabetic nephropathy. European journal of pharmacology 2020, **888**: 173574.
17. Zhou LT, Zhang ZJ, Cao JY, Chen H, Zhu YS, Wu X, *et al.* The unique molecular mechanism of diabetic nephropathy: a bioinformatics analysis of over 250 microarray datasets. Clinical kidney journal 2021, **14**(6): 1626–1638.
18. Liu H, Sridhar VS, Boulet J, Dharia A, Khan A, Lawler PR, *et al.* Cardiorenal protection with SGLT2 inhibitors in patients with diabetes mellitus: from biomarkers to clinical outcomes in heart failure and diabetic kidney disease. Metabolism: clinical and experimental 2021, **126**: 154918.
19. Ravindran S, Munusamy S. Renoprotective mechanisms of sodium-glucose co-transporter 2 (SGLT2) inhibitors against the progression of diabetic kidney disease. *Journal of cellular physiology* 2021.

20. Shin SJ, Chung S, Kim SJ, Lee EM, Yoo YH, Kim JW, *et al.* Effect of Sodium-Glucose Co-Transporter 2 Inhibitor, Dapagliflozin, on Renal Renin-Angiotensin System in an Animal Model of Type 2 Diabetes. PloS one 2016, **11**(11): e0165703.
21. Otterbein LE, Choi AM. Heme oxygenase: colors of defense against cellular stress. American journal of physiology Lung cellular and molecular physiology 2000, **279**(6): L1029-1037.
22. Dawn B, Bolli R. HO-1 induction by HIF-1: a new mechanism for delayed cardioprotection? American journal of physiology Heart and circulatory physiology 2005, **289**(2): H522-524.
23. Lok CN, Ponka P. Identification of a hypoxia response element in the transferrin receptor gene. The Journal of biological chemistry 1999, **274**(34): 24147–24152.
24. Lee PJ, Jiang BH, Chin BY, Iyer NV, Alam J, Semenza GL, *et al.* Hypoxia-inducible factor-1 mediates transcriptional activation of the heme oxygenase-1 gene in response to hypoxia. The Journal of biological chemistry 1997, **272**(9): 5375–5381.
25. Feng X, Wang S, Sun Z, Dong H, Yu H, Huang M, *et al.* Ferroptosis Enhanced Diabetic Renal Tubular Injury via HIF-1α/HO-1 Pathway in db/db Mice. Frontiers in endocrinology 2021, **12**: 626390.
26. Dong H, Qiang Z, Chai D, Peng J, Xia Y, Hu R, *et al.* Nrf2 inhibits ferroptosis and protects against acute lung injury due to intestinal ischemia reperfusion via regulating SLC7A11 and HO-1. Aging 2020, **12**(13): 12943–12959.
27. Ma H, Wang X, Zhang W, Li H, Zhao W, Sun J, *et al.* Melatonin Suppresses Ferroptosis Induced by High Glucose via Activation of the Nrf2/HO-1 Signaling Pathway in Type 2 Diabetic Osteoporosis. *Oxidative medicine and cellular longevity* 2020, **2020**: 9067610.
28. Adedoyin O, Boddu R, Traylor A, Lever JM, Bolisetty S, George JF, *et al.* Heme oxygenase-1 mitigates ferroptosis in renal proximal tubule cells. American journal of physiology Renal physiology 2018, **314**(5): F702-f714.
29. Tang Z, Ju Y, Dai X, Ni N, Liu Y, Zhang D, *et al.* HO-1-mediated ferroptosis as a target for protection against retinal pigment epithelium degeneration. Redox biology 2021, **43**: 101971.
30. Miess H, Dankworth B, Gouw AM, Rosenfeldt M, Schmitz W, Jiang M, *et al.* The glutathione redox system is essential to prevent ferroptosis caused by impaired lipid metabolism in clear cell renal cell carcinoma. Oncogene 2018, **37**(40): 5435–5450.
31. Yang M, Chen P, Liu J, Zhu S, Kroemer G, Klionsky DJ, *et al.* Clockophagy is a novel selective autophagy process favoring ferroptosis. Science advances 2019, **5**(7): eaaw2238.
32. Jiang N, Zhao H, Han Y, Li L, Xiong S, Zeng L, *et al.* HIF-1α ameliorates tubular injury in diabetic nephropathy via HO-1-mediated control of mitochondrial dynamics. Cell proliferation 2020, **53**(11): e12909.
33. Cai T, Ke Q, Fang Y, Wen P, Chen H, Yuan Q, *et al.* Sodium-glucose cotransporter 2 inhibition suppresses HIF-1α-mediated metabolic switch from lipid oxidation to glycolysis in kidney tubule cells of diabetic mice. Cell death & disease 2020, **11**(5): 390.
34. Li J, Liu H, Takagi S, Nitta K, Kitada M, Srivastava SP, *et al.* Renal protective effects of empagliflozin via inhibition of EMT and aberrant glycolysis in proximal tubules. JCI insight 2020, **5**(6).

35. Tervaert TW, Mooyaart AL, Amann K, Cohen AH, Cook HT, Drachenberg CB, *et al.* Pathologic classification of diabetic nephropathy. Journal of the American Society of Nephrology: JASN 2010, **21**(4): 556–563.
36. Marathe PH, Gao HX, Close KL. American Diabetes Association Standards of Medical Care in Diabetes 2017. Journal of diabetes 2017, **9**(4): 320–324.
37. Bolger AM, Lohse M, Usadel B. Trimmomatic: a flexible trimmer for Illumina sequence data. Bioinformatics (Oxford, England) 2014, **30**(15): 2114–2120.
38. Kim D, Langmead B, Salzberg SL. HISAT: a fast spliced aligner with low memory requirements. Nature methods 2015, **12**(4): 357–360.
39. Roberts A, Trapnell C, Donaghey J, Rinn JL, Pachter L. Improving RNA-Seq expression estimates by correcting for fragment bias. Genome biology 2011, **12**(3): R22.
40. Trapnell C, Williams BA, Pertea G, Mortazavi A, Kwan G, van Baren MJ, *et al.* Transcript assembly and quantification by RNA-Seq reveals unannotated transcripts and isoform switching during cell differentiation. Nature biotechnology 2010, **28**(5): 511–515.
41. Anders S, Pyl PT, Huber W. HTSeq–a Python framework to work with high-throughput sequencing data. Bioinformatics (Oxford, England) 2015, **31**(2): 166–169.
42. Anders S, Huber W. Differential expression analysis for sequence count data. Genome biology 2010, **11**(10): R106.
43. Kanehisa M, Araki M, Goto S, Hattori M, Hirakawa M, Itoh M, *et al.* KEGG for linking genomes to life and the environment. Nucleic acids research 2008, **36**(Database issue): D480-484.
44. Tang D, Chen X, Kang R, Kroemer G. Ferroptosis: molecular mechanisms and health implications. Cell research 2021, **31**(2): 107–125.
45. Dar HH, Tyurina YY, Mikulska-Ruminska K, Shrivastava I, Ting HC, Tyurin VA, *et al.* Pseudomonas aeruginosa utilizes host polyunsaturated phosphatidylethanolamines to trigger theft-ferroptosis in bronchial epithelium. The Journal of clinical investigation 2018, **128**(10): 4639–4653.
46. Yang WS, SriRamaratnam R, Welsch ME, Shimada K, Skouta R, Viswanathan VS, *et al.* Regulation of ferroptotic cancer cell death by GPX4. Cell 2014, **156**(1–2): 317–331.
47. Yaribeygi H, Simental-Mendía LE, Banach M, Bo S, Sahebkar A. The major molecular mechanisms mediating the renoprotective effects of SGLT2 inhibitors: An update. Biomedicine & Pharmacotherapy 2019, **120**: 109526.
48. Liu ZZ, Bullen A, Li Y, Singh P. Renal Oxygenation in the Pathophysiology of Chronic Kidney Disease. Frontiers in physiology 2017, **8**: 385.
49. Friederich-Persson M, Thörn E, Hansell P, Nangaku M, Levin M, Palm F. Kidney hypoxia, attributable to increased oxygen consumption, induces nephropathy independently of hyperglycemia and oxidative stress. *Hypertension (Dallas, Tex*: 1979) 2013, **62**(5): 914–919.
50. Dekkers CCJ, Petrykiv S, Laverman GD, Cherney DZ, Gansevoort RT, Heerspink HJL. Effects of the SGLT-2 inhibitor dapagliflozin on glomerular and tubular injury markers. Diabetes, obesity &

metabolism 2018, **20**(8): 1988–1993.

51. Chang DY, Li XQ, Chen M, Zhao MH. Dapagliflozin Ameliorates Diabetic Kidney Disease via Upregulating Crry and Alleviating Complement Over-activation in db/db Mice. Frontiers in pharmacology 2021, **12**: 729334.
52. Nayak BK, Shanmugasundaram K, Friedrichs WE, Cavaglierii RC, Patel M, Barnes J, *et al.* HIF-1 Mediates Renal Fibrosis in OVE26 Type 1 Diabetic Mice. Diabetes 2016, **65**(5): 1387–1397.
53. Hu J, Wang W, Zhang F, Li PL, Boini KM, Yi F, *et al.* Hypoxia inducible factor-1α mediates the profibrotic effect of albumin in renal tubular cells. Scientific reports 2017, **7**(1): 15878.
54. Hasegawa S, Tanaka T, Saito T, Fukui K, Wakashima T, Susaki EA, *et al.* The oral hypoxia-inducible factor prolyl hydroxylase inhibitor enarodustat counteracts alterations in renal energy metabolism in the early stages of diabetic kidney disease. Kidney international 2020, **97**(5): 934–950.
55. Sugahara M, Tanaka S, Tanaka T, Saito H, Ishimoto Y, Wakashima T, *et al.* Prolyl Hydroxylase Domain Inhibitor Protects against Metabolic Disorders and Associated Kidney Disease in Obese Type 2 Diabetic Mice. Journal of the American Society of Nephrology: JASN 2020, **31**(3): 560–577.
56. Packer M. Mechanisms Leading to Differential Hypoxia-Inducible Factor Signaling in the Diabetic Kidney: Modulation by SGLT2 Inhibitors and Hypoxia Mimetics. American journal of kidney diseases: the official journal of the National Kidney Foundation 2021, **77**(2): 280–286.
57. Lee DW, Andersen JK. Role of HIF-1 in iron regulation: potential therapeutic strategy for neurodegenerative disorders. Current molecular medicine 2006, **6**(8): 883–893.
58. Zhang X, Guan T, Yang B, Chi Z, Wan Q, Gu HF. SLC30A7 has anti-oxidant stress effects in high glucose-induced apoptosis via the NFE2L2/HMOX1 signal transduction pathway. Diabetes research and clinical practice 2021, **172**: 108445.
59. Antar SA, Abdo W, Taha RS, Farage AE, El-Moselhy LE, Amer ME, *et al.* Telmisartan attenuates diabetic nephropathy by mitigating oxidative stress and inflammation, and upregulating Nrf2/HO-1 signaling in diabetic rats. Life sciences 2021, **291**: 120260.
60. Wen Y, Liu Y, Huang Q, Liu R, Liu J, Zhang F, *et al.* Moringa oleifera Lam. seed extract protects kidney function in rats with diabetic nephropathy by increasing GSK-3β activity and activating the Nrf2/HO-1 pathway. Phytomedicine: international journal of phytotherapy and phytopharmacology 2022, **95**: 153856.
61. Sun HK, Lee YM, Han KH, Kim HS, Ahn SH, Han SY. Phosphodiesterase inhibitor improves renal tubulointerstitial hypoxia of the diabetic rat kidney. The Korean journal of internal medicine 2012, **27**(2): 163–170.
62. Chang LC, Chiang SK, Chen SE, Yu YL, Chou RH, Chang WC. Heme oxygenase-1 mediates BAY 11-7085 induced ferroptosis. Cancer letters 2018, **416**: 124–137.
63. Kwon MY, Park E, Lee SJ, Chung SW. Heme oxygenase-1 accelerates erastin-induced ferroptotic cell death. Oncotarget 2015, **6**(27): 24393–24403.
64. Dixon SJ, Lemberg KM, Lamprecht MR, Skouta R, Zaitsev EM, Gleason CE, *et al.* Ferroptosis: an iron-dependent form of nonapoptotic cell death. Cell 2012, **149**(5): 1060–1072.

65. Dixon SJ, Patel DN, Welsch M, Skouta R, Lee ED, Hayano M, *et al.* Pharmacological inhibition of cystine-glutamate exchange induces endoplasmic reticulum stress and ferroptosis. *eLife* 2014, **3**: e02523.
66. Stockwell BR, Jiang X, Gu W. Emerging Mechanisms and Disease Relevance of Ferroptosis. Trends in cell biology 2020, **30**(6): 478–490.
67. Seiler A, Schneider M, Förster H, Roth S, Wirth EK, Culmsee C, *et al.* Glutathione peroxidase 4 senses and translates oxidative stress into 12/15-lipoxygenase dependent- and AIF-mediated cell death. Cell metabolism 2008, **8**(3): 237–248.
68. Seibt TM, Proneth B, Conrad M. Role of GPX4 in ferroptosis and its pharmacological implication. Free radical biology & medicine 2019, **133**: 144–152.

Figures

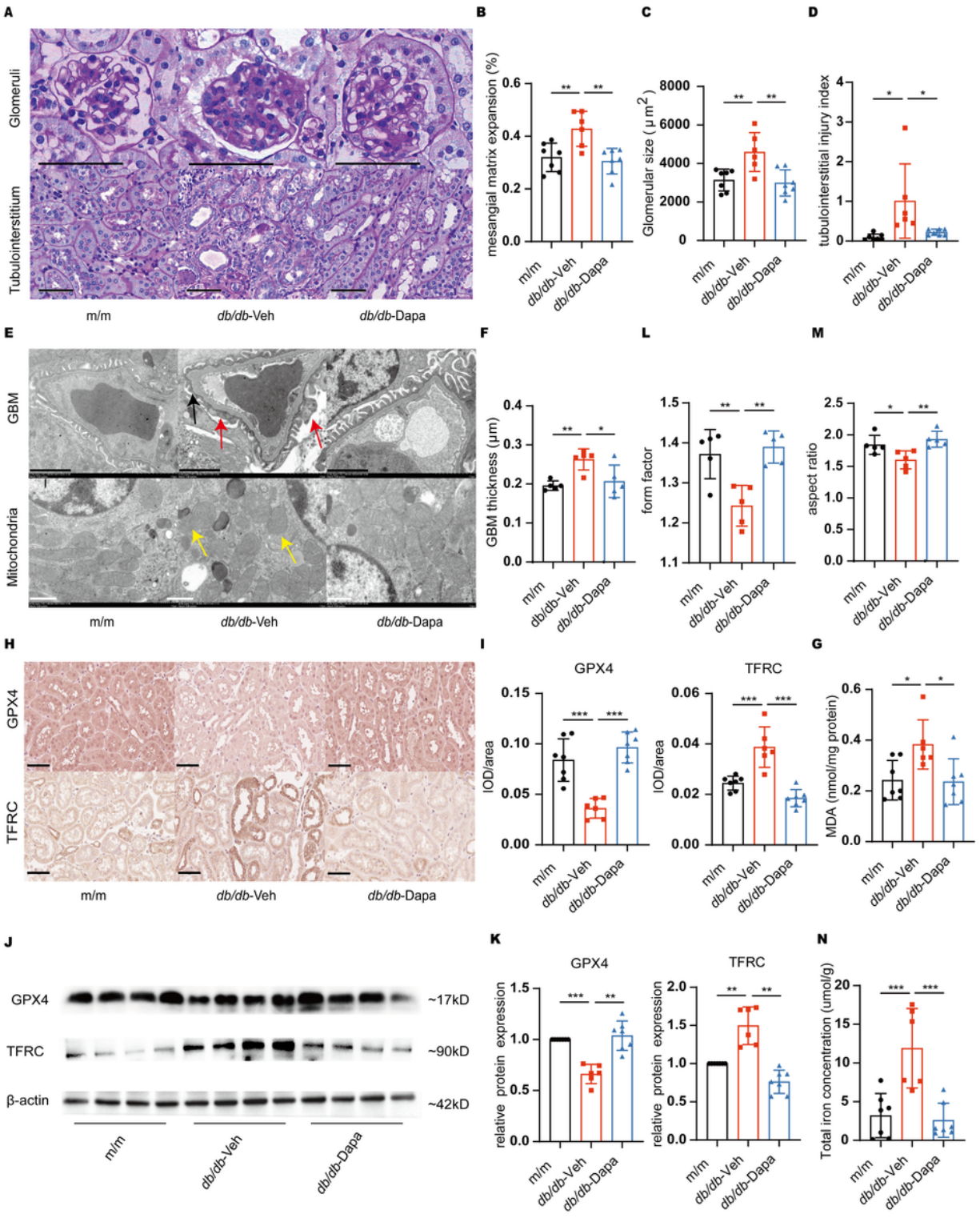

Figure 1

Dapagliflozin alleviated renal ferroptosis in *db/db* mice.

Representative light microscopy photomicrographs of glomeruli and tubulointerstitium of PAS staining kidney tissue (**A**) (scale bar=60μm), and mesangial matrix expansion (**B**), glomerular size (**C**), and tubulointerstitial lesions (**D**) were assessed. Representative transmission electron microscopy

photomicrographs of glomeruli and mitochondria morphology of kidney cortex (**E**). The black arrow indicates the increasing thickness of GBM, and the red and yellow arrows indicate the fused foot process and mitochondria with disappeared cristae. Black scale bar=2μm, and white scale bar=1μm. Quantification of mean GBM thickness (**F**). The MDA level in the kidney cortex lysates (**G**). Immunohistochemical staining results of GPX4 and TFRC in kidney cortex, and scale bar=60μm (**H**). Semi-quantification analysis of immunohistochemical staining of GPX4 and TFRC (**I**). The protein expression of GPX4 and TFRC (**J**) and semi-quantification results of gray value (**K**) in kidney cortex of mice. The form factor (**L**) and aspect ratio of mitochondria per image (**M**) in kidney tubular cells. The iron concentrations in the kidney cortex lysates (**N**). GBM, glomerular basement membrane; GPX4, glutathione peroxidase 4; IOD/area, the intensity of immunohistochemical staining; MDA, malondialdehyde; *m/m*, wild type mice; *db/db*-Veh, vehicle-treated *db/db* mice; *db/db*-Dapa, dapagliflozin-treated *db/db* mice; TFRC, transferrin receptor. Data were expressed as mean ± SD. **p*<0.05, ***p*<0.01, ****p*<0.001.

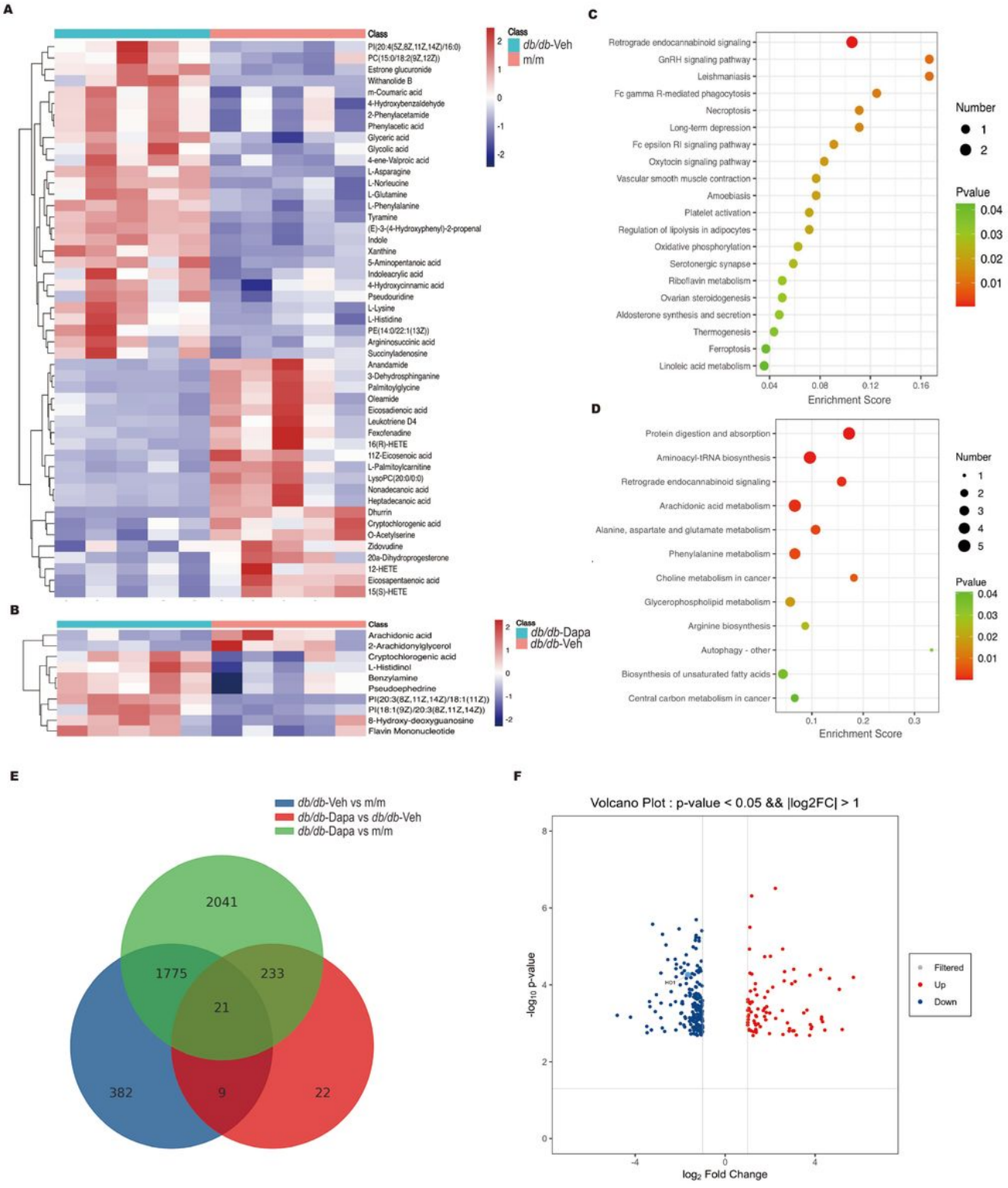

Figure 2

Ferroptosis played an important role in the renoprotective effects of dapagliflozin.

The metabolites difference between *m/m* mice and vehicle-treated *db/db* mice (**A**). The metabolites difference between vehicle-treated and dapagliflozin-treated *db/db* mice (**B**). The KEGG pathway clustering results of differential metabolites between m/m mice and vehicle-treated *db/db* mice (**C**) and

vehicle-treated and dapagliflozin-treated *db/db* mice (**D**). The intersection of differentially expressed genes in *m/m*, vehicle-treated *db/db* and dapagliflozin-treated *db/db* mice (**E**). The differentially expressed genes between vehicle-treated and dapagliflozin-treated *db/db* mice (**F**). HO1, heme oxygenase-1; m/m, wild type mice; *db/db*-Veh, vehicle-treated *db/db* mice; *db/db*-Dapa, dapagliflozin-treated *db/db* mice.

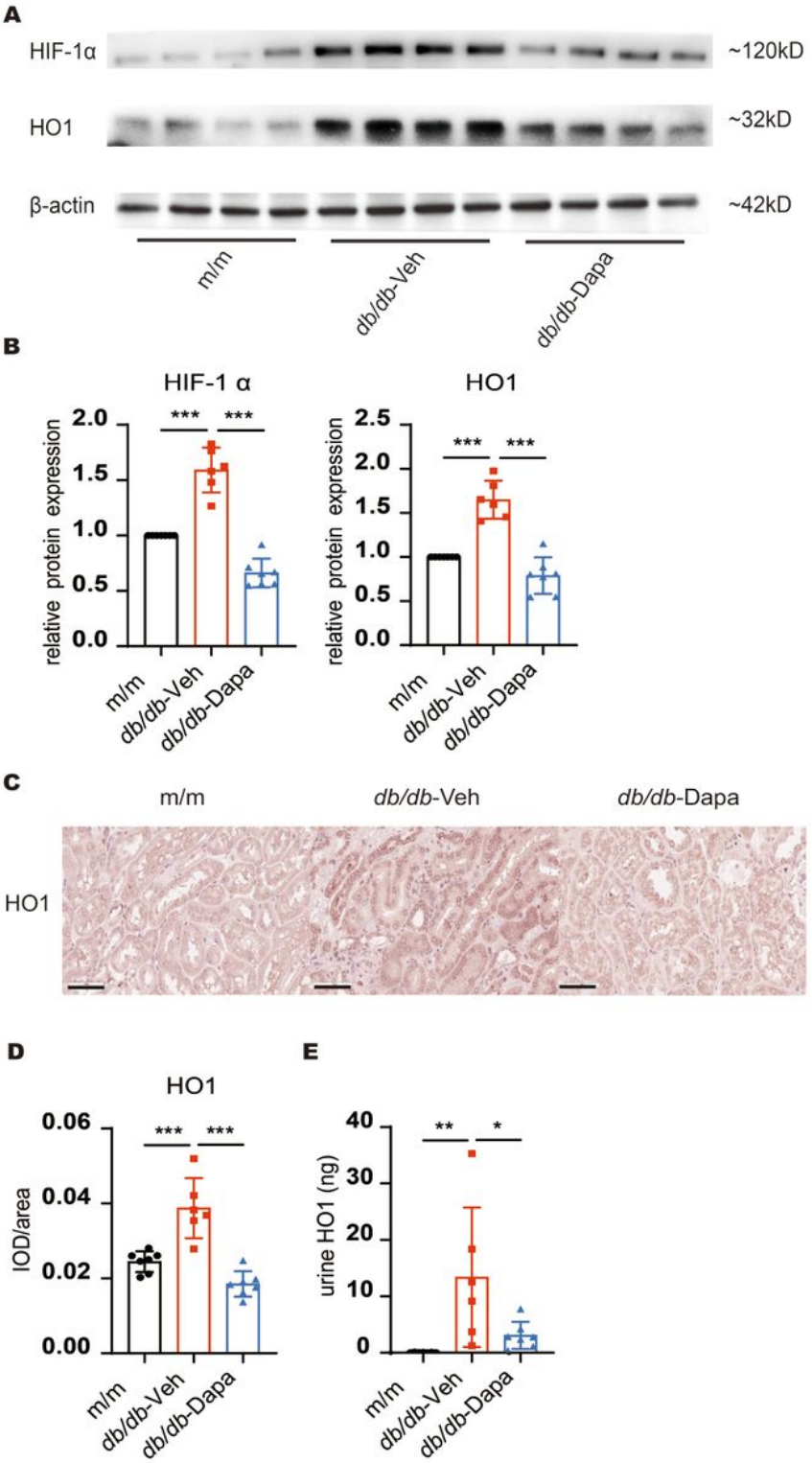

Figure 3

Dapagliflozin reversed increased expression of HIF-1α/HO1 axis in *db/db* mice.

The protein expression levels in kidney cortex lysates of m/m, vehicle-treated *db/db* and dapagliflozin-treated *db/db* mice (**A**), and semi-quantification results of gray value (**B**). Immunohistochemical staining results of HO1 in kidney cortex, and scale bar=60μm (**C**). Semi-quantification analysis of the HO1 level in immunohistochemical staining (**D**). The urine HO1 level of m/m, vehicle-treated *db/db* and dapagliflozin-treated *db/db* mice (**E**). HIF-1α, hypoxia-inducible factor-1α; HO1, heme oxygenase-1; IOD/area, the intensity of immunohistochemical staining; m/m, wild type mice; *db/db*-Veh, vehicle-treated *db/db* mice; *db/db*-Dapa, dapagliflozin-treated *db/db* mice. Data were expressed as mean ± SD. **p*<0.05, ***p*<0.01, ****p*<0.001.

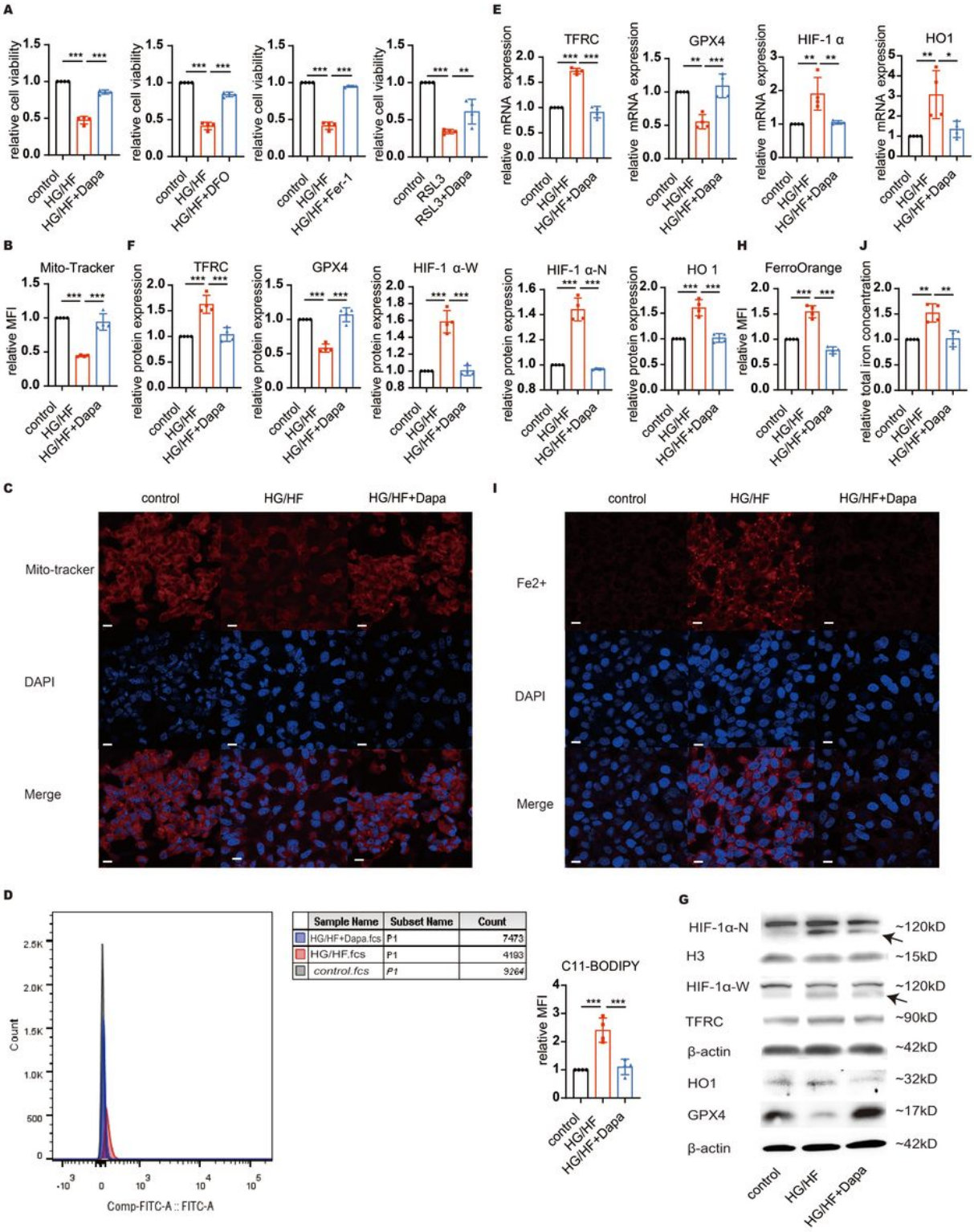

Figure 4

Dapagliflozin rescued the ferroptosis induced by HG/HF by downregulating HIF-1α/HO1 axis in HK-2 cells.

The viability of HK-2 cells cultured in the media with dapagliflozin, deferoxamine mesylate, ferrostatin-1 for 72h, or RSL3 for 48h (**A**). Detection of mitochondrial activity in HK-2 cells treated with different

treatments for 72h using confocal laser scanning microscope (scale bar =10μm) (**C**), and the relative MFI of PE channel was also calculated using FACS (**B**). Lipid peroxidation level of HK-2 cells in different treatments assessed by C11-BODIPY$^{581/591}$ using FACS and relative MFI of FITC channel was calculated (**D**). The mRNA expression levels of TFRC, GPX4, HIF-1α and HO1 in each group (**E**). The protein expression levels of TFRC, GPX4, HIF-1α and HO1 in whole cell lysates and HIF-1α in nuclear lysates of each group (**G**) and semi-quantitative analysis of gray value (**F**). Detection of Fe^{2+} in HK-2 cells treated with different treatments for 72h using confocal laser scanning microscope (scale bar =10μm) (**I**), and the relative MFI of PE channel was also calculated using FACS (**H**). Total iron level of HK-2 cells in different treatments (**J**). Dapa, dapagliflozin; DFO, deferoxamine mesylate; Fer-1, ferrostatin-1; GPX4, glutathione peroxidase 4; HIF-1α, hypoxia-inducible factor-1α; HIF-1α-N, HIF-1α in nuclear lysates; HIF-1α-W, HIF-1α in whole cell lysates; HG/HF, high glucose/high fat; HO1, heme oxygenase-1; MFI, mean fluorescent intensity; TFRC, transferrin receptor. Data were expressed as mean ± SD. *p<0.05, **p<0.01, ***p<0.001.

Figure 5

Inhibition of HIF-1α/HO1 axis alleviated the ferroptosis induced by HG/HF in HK-2 cells.

The protein expression levels of TFRC, GPX4, HIF-1α and HO1 in whole cell lysates and HIF-1α in nuclear lysates of each group of cells (**B**) and semi-quantitative analysis of gray value (**A**). The viability of HK-2 cells being cultured in the media with different treatments for 72h (**C**). Detection of mitochondrial activity in HK-2 cells treated with different treatments for 72h using confocal laser scanning microscope (scale bar=10μm) (**E**), and the relative MFI of PE channel was also calculated using FACS (**D**). The mRNA expression levels of TFRC and GPX4 in each group (**F**). Total iron concentration of HK-2 cells in different treatments (**G**). Detection of Fe^{2+} in HK-2 cells treated with different treatments for 72h using confocal laser scanning microscope (scale bar=10μm) (**I**), and the relative MFI of PE channel was also calculated using FACS (**H**). Lipid peroxidation levels of HK-2 cells in different treatments assessed by C11-BODIPY$^{581/591}$ using FACS and relative MFI of FITC channel was calculated (**J**). Dapa, dapagliflozin; DMOG, dimethyloxallyl glycine; GPX4, glutathione peroxidase 4; HIF-1α, hypoxia-inducible factor-1α; HIF-1α-N, HIF-1α in nuclear lysates; HIF-1α-W, HIF-1α in whole cell lysates; HG/HF, high glucose/high fat; HO1, heme oxygenase-1; MFI, mean fluorescent intensity; TFRC, transferrin receptor; Znpp, zinc protoporphyrin. Data were expressed as mean ± SD. *p<0.05, **p<0.01, ***p<0.001.

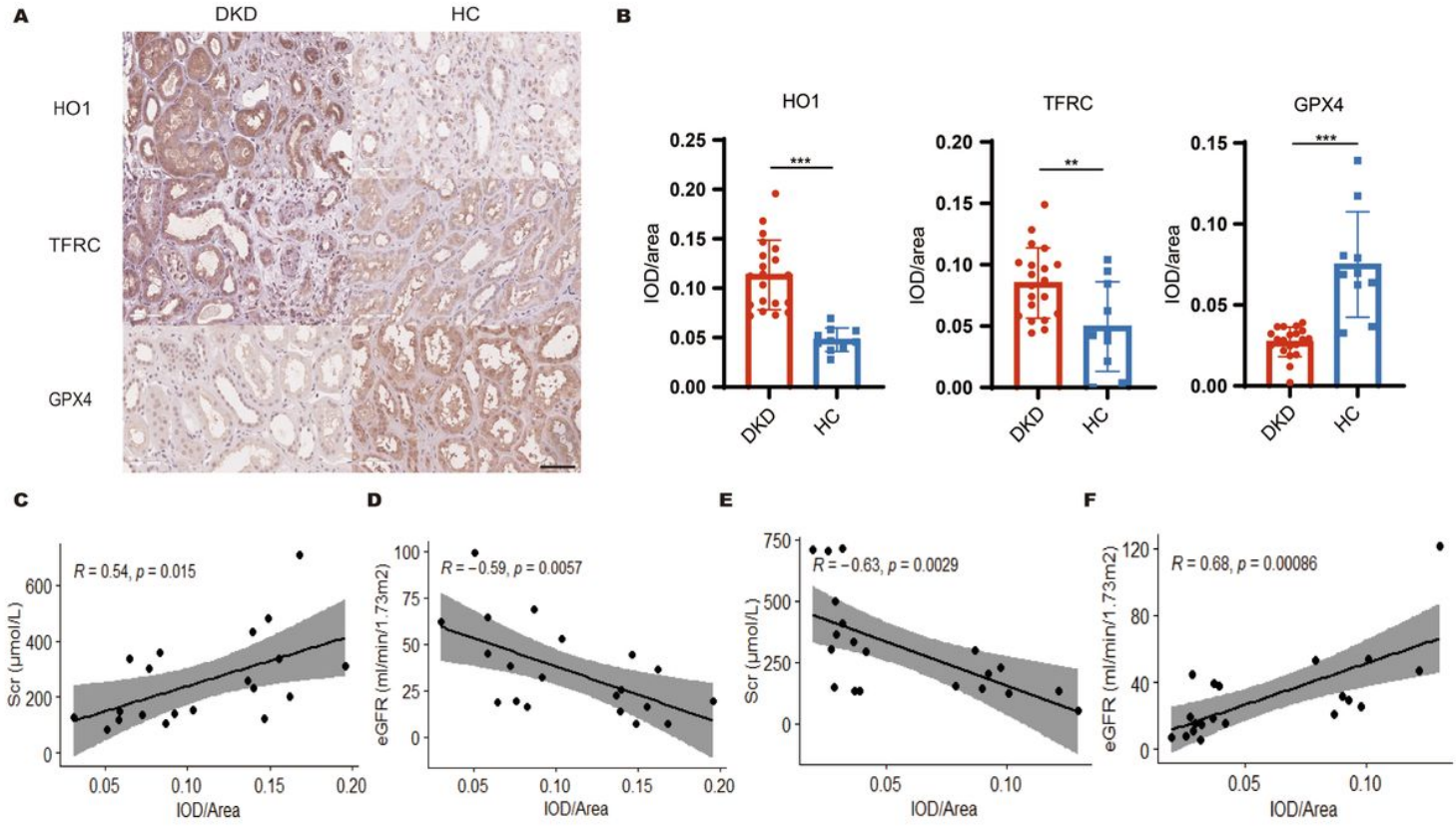

Figure 6

Ferroptosis significantly elevated in kidney samples of DKD patients.

Immunohistochemical staining results of HO1, GPX4 and TFRC in kidney sections of DKD patients and HC, and scale bar=60μm (**A**). Semi-quantification analysis of immunohistochemical staining of HO1, GPX4 and TFRC (**B**). The correlation of HO1 and clinical parameters of DKD patients including Scr (**C**) and eGFR (**D**). The correlation of GPX4 and clinical parameters of DKD patients including Scr (**E**) and eGFR (**F**). DKD, diabetic kidney disease; eGFR, estimated glomerular filtration rate; GPX4, glutathione peroxidase 4; HC, healthy control; HO1, heme oxygenase-1; IOD/area, the intensity of immunohistochemical staining; Scr, serum creatinine; TFRC, transferrin receptor. Data were expressed as mean ± SD. *p<0.05, **p<0.01, ***p<0.001.

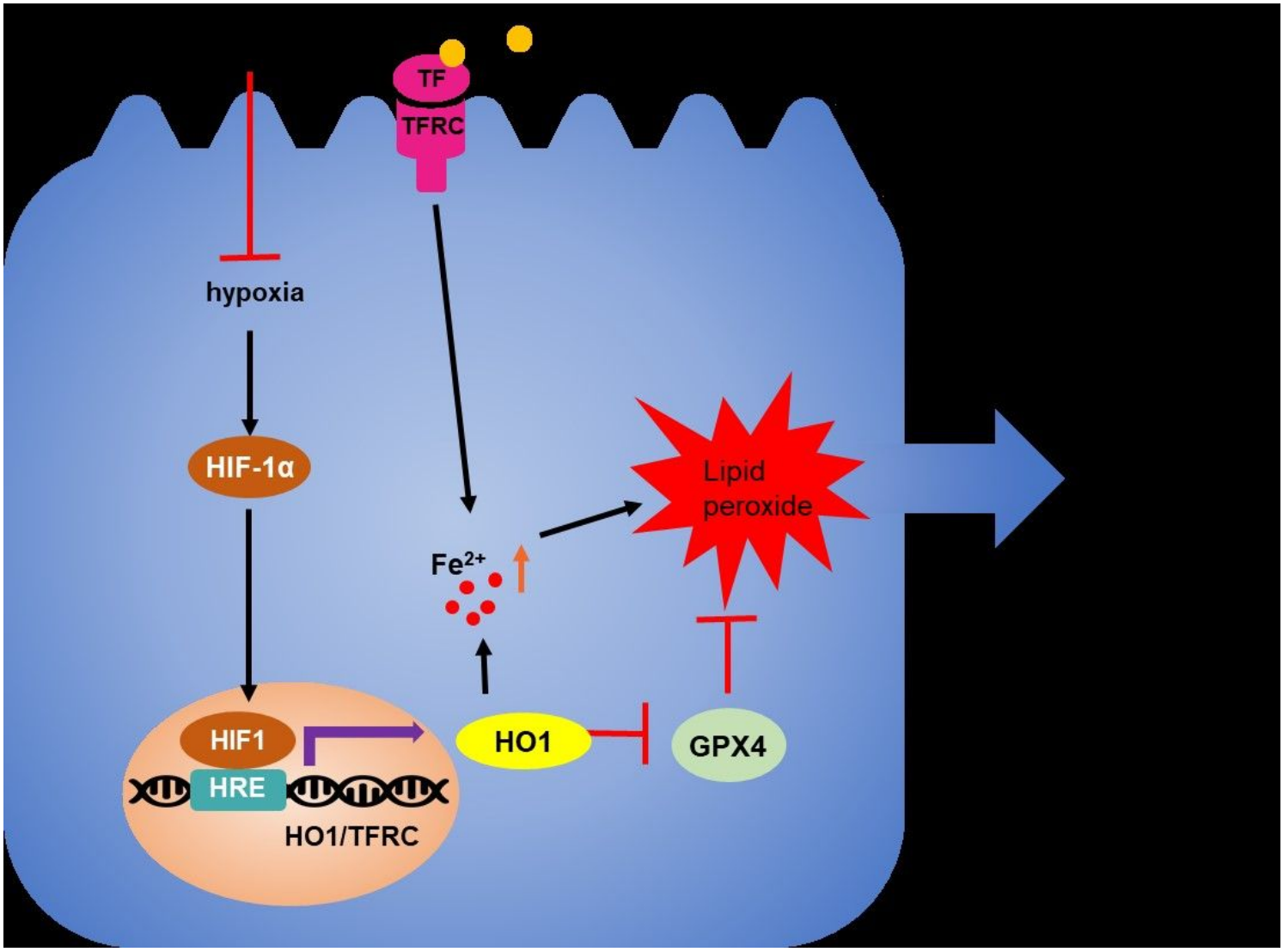

Figure 7

The proposed model of dapagliflozin in DKD alleviation.

GPX4, glutathione peroxidase 4; HIF-1α, hypoxia-inducible factor-1α; HRE, hypoxia response element; SGLT2i, sodium-glucose cotransporter 2 inhibitors; TF, transferrin; TFRC, transferrin receptor.

Supplementary Files

This is a list of supplementary files associated with this preprint. Click to download.

- SupplementalMaterial.pdf
- SupplementalMaterial2.pdf